# Hydraulic/partitioning tracer tomography for characterization of dense nonaqueous phase liquid source zones

Tian-Chyi J. Yeh[1,2] and Junfeng Zhu[1]

Received 10 January 2006; revised 23 February 2007; accepted 13 March 2007; published 30 June 2007.

[1] A new technology, hydraulic/partitioning tracer tomography (HPTT), is proposed to survey spatial distributions of hydraulic properties and dense nonaqueous phase liquids (DNAPLs) in the subsurface. HPTT is nothing more than a set of multiple hydraulic/partitioning tracer tests and synthesis of all the tests to map the spatial distributions. It involves injection of water at one borehole in a source zone to create a steady state forced gradient flow field, then release of conservative/partitioning tracers at the same borehole, and monitoring heads and tracer breakthroughs at the others. The same operation is repeated using different boreholes for the water and the tracer injections. To analyze the head and tracer data obtained from the proposed tomographic survey, a joint stochastic estimator was developed. Numerical experiments were then conducted to evaluate the effectiveness of HPTT as well as the stochastic estimator. Results show that prior knowledge of hydraulic heterogeneity is critical for mapping the distribution of DNAPLs. In addition, the results suggest that the proposed HPTT in conjunction with the stochastic estimator is potentially a viable tool for high-resolution characterization of subsurface heterogeneity and contamination.

**Citation:** Yeh, T.-C. J., and J. Zhu (2007), Hydraulic/partitioning tracer tomography for characterization of dense nonaqueous phase liquid source zones, *Water Resour. Res.*, *43*, W06435, doi:10.1029/2006WR004877.

## 1. Introduction

[2] Dense nonaqueous phase liquids (DNAPLs) are prevalent at a large number of sites throughout the world. The high densities, low interfacial tensions, and low viscosities of halogenated solvents can lead to deep DNAPL penetration (*Pankow and Cherry*, 1996). In porous media, much of the DNAPL mass remains in the subsurface as persistent source zones. Without remediation, these source zones can contribute to long-term groundwater contamination for decades to centuries. Therefore the spatial distribution, mass, and composition of DNAPLs present in the source zone need to be characterized in great detail so that efficient remediation schemes can be designed and accomplished.

[3] Recent studies by *Rao et al.* [2000] and *Khachikian and Harmon* [2000] suggested that our knowledge of DNAPL dissolution and remediation issues has matured, and they underlined the importance of heterogeneity in characterizing DNAPL spatial distributions. In particular, *Khachikian and Harmon* [2000] emphasized that ''inverse modeling efforts aimed at exploiting the previous developments should be expanded to support field-scale characterization of DNAPL location and strength as a dissolving source.''

[4] To our knowledge, there are few publications on inverse modeling efforts to obtain estimations of spatial distribution of DNAPL in the subsurface. *Sciortino et al.* [2000] developed an inverse model to locate DNAPL pools. *James et al.* [2000] used a stochastic method to estimate spatial distribution of DNAPL residual content from partitioning tracer breakthrough curve moments. Extending the work by *James et al.* [1997], *Zhang and Graham* [2001] presented an extended Kalman filter for estimating spatially distributed residual saturation of DNAPL and the Darcy flux using a partitioning tracer plume in a three-dimensional heterogeneous aquifer. Their results are exciting, and the algorithm is promising. But using 420 sampling locations (84 multilevel samplers with 5 samples at 5 evenly spaced vertical locations) out of a total of 686 elements (98 elements in the horizontal plane and 7 elements in the vertical) of the simulation domain is highly idealized. Nevertheless, *Zhang and Graham* [2001] demonstrated that it is theoretically feasible to estimate a residual DNAPL distribution using an inverse approach. *Datta-Gupta et al.* [2002] employed a streamline-based inverse approach to analyze interwell partition tracer tests for estimating three-dimensional spatial variation of DNAPL saturation.

[5] Besides using simplified assumptions (such as the porosity or water content is spatially invariant and known) and estimating DNAPL saturations only, most previous inverse efforts did not consider the hydrologic site characterization prior to a partitioning tracer test nor did they take advantage of the hydraulic head information created during the test. Field studies [i.e., *Mas-Pla et al.*, 1992; *Yeh et al.*, 1995a] however showed that a detailed three-dimensional characterization of the hydraulic conductivity field indisputably improved the prediction of chloride tracer migration in a coastal sandy aquifer. Later, *McCarthy et al.* [1996] proved that the well-characterized migration paths of the

[1]Department of Hydrology and Water Resources, The University of Arizona, Tucson, Arizona, USA.
[2]Also at Department of Resources Engineering, National Chen-Kung University, Tainan, Taiwan.


0043-1397/07/2006WR004877$09.00

chloride tracer led to a better understanding of migration and chemical processes of natural organic matters in the same aquifer. Similarly, using conditional simulations, *Harter and Yeh* [1996] reported that predictions conditioned with observed hydraulic heads yielded more accurate tracer migration paths. These findings lead us to believe that a characterization of subsurface heterogeneity prior to partitioning tracer tests or taking advantage of hydraulic head observations during the tests to characterize the subsurface will facilitate a better delineation of DNAPL distribution.

[6] Over the past few decades, mapping aquifer heterogeneity generally has relied on either local small-scale tests (e.g., core samples, aquifer, and slug tests) or large-scale tests (i.e., inverse modeling using sparse hydraulic head measurements in a field site, and geophysical surveys). Small-scale field tests, in general, are costly, destructive to the field site, and perhaps physically prohibitive if a detailed three-dimensional heterogeneity distribution of a field site is required. Moreover, *Beckie and Harvey* [2002] questioned the representativeness of the properties estimated from slug tests, and *Wu et al.* [2005] cast doubt on the validity of applications of the classical analysis for aquifer tests to heterogeneous aquifers. Similarly, traditional inverse modeling efforts to obtain spatially distributed parameters of aquifers often results in subjective site characterization because of insufficient data. On the other hand, geophysical surveys often produce images of the geophysical properties of the subsurface, which are difficult to be translated into the hydraulic properties that are pertinent to modeling of flow and solute transport processes.

[7] In addition to using sparse hydraulic head data, hydrologists have exploited solute concentration data to estimate the hydraulic conductivity field. For example, *Harvey and Gorelick* [1995] estimated a hydraulic conductivity field using measurements of hydraulic conductivity, head, and solute arrival time. They found that the use of arrival time and the use of head data provided different but complementary information about the large-scale features of the hydraulic conductivity fields. Using cokriging, *Li and Yeh* [1999] estimated the hydraulic conductivity field of variably saturated media using pressure head, solute concentration, and solute arrival time measurements. Steady state head measurements were found to be most effective among the three types of measurements while solute concentration data was found to slightly enhance the estimates based on head measurements alone. *Cirpka and Kitanidis* [2001] used the first temporal moments of solute data to estimate the hydraulic conductivity field. They recommended the use of both head and tracer arrival-time data for inverse modeling because arrival-time data are very sensitive to the hydraulic conductivities along a narrow strip upstream of the measurement location, whereas hydraulic heads are influenced from hydraulic conductivities in all directions.

[8] Recently, a new technology, hydraulic tomography (HT), has been developed [e.g., *Gottlieb and Dietrich*, 1995; *Renshaw*, 1996; *Vasco et al.*, 2000; *Yeh and Liu*, 2000; *Bohling et al.*, 2002; *McDermott et al.*, 2003; *Brauchler et al.*, 2003; *Zhu and Yeh*, 2005, 2006; and others] to provide high-resolution aquifer characterization. In simple terms, HT is a sequential cross-hole hydraulic test followed by inversion of all the data to map the spatial distribution of aquifer hydraulic properties. Specifically, HT involves installation of multiple wells in an aquifer, which are partitioned into several intervals along the depth using packers. A sequential aquifer test at selected intervals is then conducted. During the test, water is injected or withdrawn (i.e., a pressure excitation) at a selected interval in a given well. Pressure responses of the subsurface are then monitored at other intervals at this well and other wells. This test produces a set of pressure excitation/response data of the subsurface. Once a test is completed, the pump is moved to another interval and the test is repeated to collect another set of data. The same procedure is then applied to the intervals at other wells. Afterward, the data sets from all tests are processed by a mathematical model to estimate the spatial distribution of hydraulic properties of the aquifer. In essence, a set of pressure data due to one pressure excitation in a HT test is equivalent to a snapshot of the subsurface heterogeneity illuminated by a light at the excitation location. Repeating the test at a different interval is the same as taking the snapshot with a light source at a different location. The inverse model is merely an algorithm that synthesizes all the snapshots to portray a three-dimensional distribution of a hydraulic property in the test area.

[9] Using sandbox experiments and an HT analysis algorithm (sequential successive linear estimator (SSLE) by *Yeh and Liu* [2000]), *Liu et al.* [2002] demonstrated that steady state HT is an effective technique for depicting the hydraulic conductivity heterogeneity with only a limited number of invasive observations. Recently, *Zhu and Yeh* [2005, 2006] extended SSLE for steady state HT to transient HT. While both steady and transient HT surveys remain to be fully assessed in the field, there are some encouraging results from recent sandbox experiments for transient HT [*Liu et al.*, 2007]. Not only did transient HT identify the pattern of the hydraulic conductivity heterogeneity but also the variation of specific storage values in the sandbox. More interestingly, *Liu et al.* [2007] using the estimated fields successfully predicted the observed drawdown as a function of time of an independent aquifer test. Likewise, a recent application of HT to a well field at Montalto Uffugo Scalo, Italy, produced an estimated transmissivity field that is deemed consistent with the geology of the site [*Straface et al.*, 2007]. HT thus appears to be a potentially viable high-resolution aquifer characterization technology.

[10] In this paper, we propose a hydraulic/partitioning tracer tomography (HPTT) concept that integrates recent advances in characterization of DNAPLs and hydraulic heterogeneity and develop a mathematical algorithm based on this concept to estimate the spatial distributions of the hydraulic conductivity, water content, and DNAPL content in aquifers. The algorithm adopted a stochastic information fusion concept [*Yeh and Šimůnek*, 2002] such that HT complements the partitioning tracer tomography. In the subsequent parts of this paper, we introduce the concept of HPTT in section 2 and present the algorithm that analyzes data from HPTT in order to estimate hydraulic conductivity, water content, and DNAPL content using head and tracer concentration data in section 3. Numerical experiments then follow in regard to (1) the validation of the algorithm, (2) the exploration of the importance of hydraulic heterogeneity and tracer tomography, and (3) the effectiveness of HPTT for characterizing a DNAPL source zone

(section 4). Finally, discussion and conclusions are presented in section 5.

## 2. General Concept of Hydraulic/Partitioning Tracer Tomography

[11] According to the assessment of current technologies in section 1, partitioning tracers appear to be effective tracers for detecting DNAPLs. The conventional interwell partitioning tracer test and inverse modeling techniques are promising technologies to delineate residual DNAPL distributions in the subsurface. But they require densely distributed multilevel samplers [*Sillan et al.*, 1998], and they have ignored potentially useful hydraulic head data during the test and prior knowledge of hydraulic heterogeneity. As a result, development of a more effective test technologies and analysis methodologies for DNAPL source zone characterization is needed.

[12] To take on this challenge, a new technology, HPTT, is proposed. Consider a DNAPL source zone in an aquifer. First, several wells are emplaced in the source zone, and each well is partitioned into many intervals along the depth. Then, a HT survey (see introduction) is conducted, using injection of water as the source of excitation at a selected interval. After a steady, spherically divergent flow field is established, a nonreactive and a partitioning tracer are introduced at the injection interval. Breakthrough curves (BTCs) of these tracers are collected at other intervals at all wells, basically, a conventional interwell partitioning tracer test. This tracer test is then sequentially applied to other selected injection intervals in the well field, and BTCs are monitored at others. Such a sequential tracer test at different locations is called partitioning tracer tomography (PTT) and the combination of HT and PTT constitutes our HPTT. The HPTT test aims at generating many sets of pressure excitation/responses and tracer injection/BTCs using only a limited number of wells.

[13] The rationale behind the PTT is identical to that of HT with the exception that tracer injection is used as the excitation source and BTCs are the responses. Injection of water and the dual tracers at a different interval forces the tracers to travel through different portions of the source zone. Since the partitioning tracer is assumed to react with DNAPLs only, retardation of the BTC of the partitioning tracer then suggests existence of DNAPLs along the travel path. PTT therefore can detect DNAPLs in the source zone from different locations, directions, and angles. Mathematically, the BTCs resulting from different injections yield many pieces of nonredundant information about the DNAPL spatial distribution. Accordingly, the inversion of PTT becomes better constrained than that of the conventional single interwell partitioning tracer test. An appropriate analysis of the BTCs from PTT can thus yield a more detailed image of the DNAPL spatial distribution than the conventional interwell test.

[14] The BTCs are affected by both spatial distribution of DNAPLs and hydraulic heterogeneity at various scales as well as by other factors [*Rao et al.*, 2000]. The proposed HPTT takes advantage of the HT test to remove partial effects of hydraulic heterogeneity at large scales on the BTCs. The nonreactive tracer test is designed to exclude the effects of porosity and heterogeneity at small scales, since tracer samples different volumes of the medium compared with those sampled by pressure. Analysis of HT and nonreactive tracer data thus identifies the tracer migration paths with great certainty. Subsequent use of the partitioning tracer BTCs will result in the estimate of DNAPLs distribution. The estimate based on HPTT thereby would provide more information about the DNAPL distribution than that based on conventional partitioning tracer tests alone.

## 3. Mathematical Models

[15] In this section, we present the mathematical algorithm for analyzing data collected from the proposed HPTT. Specifically, we present the development of a forward model for simulation of groundwater flow and tracer transport (section 3.1); the development of a SSLE that estimates the hydraulic conductivity, water content, and DNAPL distributions (section 3.2); evaluation of covariance and cross covariance required for SSLE (section 3.3); and finally, evaluation of the sensitivities used in the determination of the covariance and cross covariance (section 3.4).

### 3.1. Governing Equations

[16] During the proposed HPTT, the forced gradient flow is steady and is assumed to be described by

$$\nabla \cdot [K(\mathbf{x})\nabla H] + Q(\mathbf{x}_k) = 0 \tag{1}$$

subject to boundary conditions:

$$H|_{\Gamma_1} = H_1, \qquad [K(\mathbf{x})\nabla H] \cdot \mathrm{n}|\Gamma_2 = q_h, \tag{2}$$

where $H$ is the total head, $\mathbf{x}$ is the spatial coordinates ($\mathbf{x} = \{x_1, x_2, x_3\}$, where $x_3$ represents the vertical coordinate and is positive upward). The term $Q(\mathbf{x}_k)$ is the pumping rate per unit volume of the aquifer at the location $\mathbf{x}_k$. The spatially varying saturated hydraulic conductivity field for water is denoted by $K(\mathbf{x})$, which includes effects of the presence of DNAPLs. Also, we assume that DNAPLs are at residual levels such that they cannot be mobilized by the flow. Equation (1) as such is considered adequate for our study. Otherwise, a multiphase flow model is necessary. In equation (2), $H_1$ denotes the prescribed total head at Dirichlet boundary $\Gamma_1$, $q_h$ is the specific discharge at Neumann boundary $\Gamma_2$, and $\mathbf{n}$ is a unit vector normal to the boundary.

[17] Transport of the conservative or partitioning tracer in this forced gradient field is assumed to be described by a general advection-dispersion-retardation equation:

$$\frac{\partial}{\partial t}(\theta_w c + K_N \theta_n c) = -\nabla \cdot (\mathbf{q}c) + \nabla \cdot (\theta_w \mathbf{D}\nabla c) + Q(\mathbf{x}_k) c_n N(\mathbf{x} - \mathbf{x}_k)(t - t_b) \tag{3}$$

subject to following initial and boundary conditions:

$$c|_{t=0} = c_0 \tag{4}$$

$$c|_{\Gamma_1} = c_1 \tag{5}$$

$$\mathbf{q}c - \theta_w \mathbf{D}\nabla c|_{\Gamma_2} = \mathbf{q}_s \tag{6}$$

where $c$ is the concentration of the conservative or partitioning tracer; $\theta_w$ is the volumetric water content (called water content, hereafter); $K_N$ is the partitioning coefficient (it is 0 if the tracer is conservative); and $\theta_n$ is the volumetric DNAPL content (called DNAPL content, hereafter). Note that the porosity is the sum of water content and DNAPL content (i.e., $\theta = \theta_w + \theta_N$). $\mathbf{q}$ is the specific discharge vector given by

$$q_i = -K\frac{\partial H}{\partial x_i}. \qquad i = 1, 2, \text{ and } 3. \tag{7}$$

In equation (3), $\mathbf{D}$ is dispersion tensor and is given as

$$D_{ij} = \frac{v_i v_j}{|\mathbf{v}|}(\alpha_L - \alpha_T) + \delta_{ij}(\alpha_T v + D_d^*) \tag{8}$$

where $\alpha_L$ and $\alpha_T$ are the longitudinal and transverse dispersivity, respectively; $v_i$ is the linear average velocity defined as $q_i / \theta_w$; $|\mathbf{v}|$ is the magnitude of the seepage velocity; $\delta_{ij}$ is the Kronecker delta function which equals unity if the indices are identical and 0 otherwise; and $D_d^*$ is the molecular diffusivity. In addition, $c_n$ is the concentration of the injected tracer solution; $N(\mathbf{x} - \mathbf{x}_k)(t - t_b)$ is a Dirac delta function which equals unity at location $\mathbf{x}_k$ at time equal to $t_b$ (the time when the tracer is released) and 0 otherwise. Moreover, $c_0$ is the initial tracer concentration; $c_1$ is the prescribed concentration at the Dirichlet boundary $\Gamma_1$; $\mathbf{q}_s$ is the tracer flux at the Neumann boundary, $\Gamma_2$. These flow and solute transport equations are solved by a three-dimensional finite element and modified method of characteristic approach (MMOC3) developed by *Srivastava and Yeh* [1992]. Formulation of equations (1)–(8) assumes that the partitioning process between groundwater and DNAPL is an ideal behavior (i.e., equilibrium partitioning).

### 3.2. SSLE Method

[18] SSLE is a stochastic estimator that seeks effective mean parameter fields of a system (i.e., an aquifer), conditioned on available primary information (i.e., measurements of system parameters), and secondary information (i.e., measurements of aquifer responses), according to spatial covariance functions of parameters (i.e., geologic structures) and physical processes. It is similar in philosophy to the quasi-linear geostatistical inverse model by *Kitanidis* [1995] and his colleagues [e.g., *Cirpka and Kitanidis*, 2001] but different in implementation; it evolves from the iterative cokriging-like algorithm by *Yeh et al.* [1995b]. It iterates to update the estimate using the same measurement rather than a new measurement as in the Kalman filter [e.g., *Zhang and Graham*, 2001]. We adopted SSLE in this study to estimate $K$, $\theta_w$, and $\theta_N$ fields using data sets collected from HPTT. The major steps of SSLE for analyzing head and concentration data from HPTT are summarized below. A detailed description of SSLE can be found in previously cited works by *Yeh et al.* [1996].

[19] First, a geologic medium under investigation is defined as a system. The hydraulic conductivity, water content, or DNAPL content distributions of the medium are then considered as the parameter fields of the system. Because of spatial variability of the parameter fields, as well as their uncertainty due to our incomplete sampling, the natural logarithms of the parameter fields, $\chi_\ell(\mathbf{x})$ (i.e., $\chi_1(\mathbf{x}) = \ln K$; $\chi_2(\mathbf{x}) = \ln \theta_w$; $\chi_3(\mathbf{x}) = \ln \theta_N$) are represented as stochastic processes. Each natural log of the stochastic parameter fields is expressed as a combination of mean $\bar{\chi}_\ell(\mathbf{x})$ and perturbation $\zeta(\mathbf{x})$ (i.e., $\ln \chi_\ell(\mathbf{x}) = \bar{\chi}_\ell(\mathbf{x}) + \zeta_\ell(\mathbf{x})$). Likewise, the responses of the system, $\phi_\alpha(\mathbf{x})$, (the subscript $\alpha$ is the index denoting the hydraulic head or the tracer concentration) induced by a tomographic test are conceptualized as stochastic processes. Each of them is expressed in terms of a mean $\bar{\phi}_\alpha(\mathbf{x})$ and a perturbation, $\varepsilon_\alpha(\mathbf{x})$, such that $\phi_\alpha(\mathbf{x}) = \bar{\phi}_\alpha(\mathbf{x}) + \varepsilon_\alpha(\mathbf{x})$.

[20] The SSLE algorithm for HPTT first analyzes data from HT to estimate the $K$ field and then the PTT data to map both $\theta_w$ and $\theta_N$ distribution. The general procedure for the HT and the PTT analysis are identical. Both involve eight major steps, which are described as follows.

[21] **Step 1**. Using antilog of $\bar{\chi}_\ell(\mathbf{x})$ (mean parameter fields), one solves equation (1) (if this is an HT analysis) or equation (3) (if PTT analysis) for the first-order approximation of mean responses of the system induced by the first excitation. The differences between the simulated mean system responses and observed responses are then evaluated at sample locations.

[22] **Step 2**. These differences, in conjunction with measured parameter perturbations, are subsequently used in classical cokriging (i.e., a multivariate linear estimator) to yield linear estimates of conditional mean log parameter fields. That is,

$$\hat{\chi}_\ell(\mathbf{x}_k) = \bar{\chi}_\ell(\mathbf{x}_k) + \sum_{i=1}^{n} \lambda_{ki}\zeta_\ell(\mathbf{x}_i) + \sum_{j,t,p}^{nw,nt,np} \beta_{kjtp}\varepsilon_\alpha(\mathbf{x}_j, t, p) \tag{9}$$

where $\hat{\chi}_\ell(\mathbf{x}_k)$ represents the estimated parameter in the log space at location, $\mathbf{x}_k$; $\lambda_{ki}$ is the weight representing the contribution to the estimate $\hat{\chi}_\ell(\mathbf{x}_k)$ from $\varsigma_\ell(\mathbf{x}_i)$ (the perturbation of the parameter sampled at location $\mathbf{x}_i$); and $n$ is the total number of samples. $\varepsilon_\alpha$ ($\mathbf{x}_j$, $t$, $p$) denotes the perturbation of the system response recorded at location $\mathbf{x}_j$ at time $t$ due to the excitation at location $p$. The weight $\beta_{kjtp}$ represents the contribution of this observed response to the estimate. The total number of observation locations is $nw$ while the total number of sampling times is represented by $nt$, whereas $np$ denotes the total number of excitations. The weights in equation (9) are determined on the basis of the spatial covariances of parameters, temporal and spatial covariances of responses, as well as the cross covariance between parameters and responses. Note that for HT, the flow is steady and time is not involved. A first-order analysis is used to derive the covariances and the cross covariances (see section 3.3).

[23] **Step 3**. Update the covariances of the parameter fields to their conditional (or residual) covariances to reflect the effects of inclusion of the observed data in step 2.

[24] **Step 4**. Since cokriging is a linear estimator, the cokriged fields are not optimal. Therefore equation (1) or

equation (3) is solved again with the newly estimated conditional mean parameter fields for new conditional mean system responses.

[25] **Step 5**. Using a linear estimator with the difference between the newly simulated conditional mean responses and the observed responses, new estimates are obtained:

$$\hat{\chi}_\ell^{(r+1)}(\mathbf{x}_k) = \hat{\chi}_\ell^{(r)}(\mathbf{x}_k) + \sum_{jtp} \omega_{kjtp}^{(r)} \left[ \phi_{\text{obs}}^{(r)}(\mathbf{x}_j, t, p) - \hat{\phi}^{(r)}(\mathbf{x}_j, t, p) \right] \tag{10}$$

where the superscript $r$ is the iteration index. The parameter field determined from step 2 is designated by $\hat{\chi}_\ell^{(r=1)}$. The weights, $\omega_{kjtp}^{(r)}$, of the new estimator are determined from the conditional covariances of the new system responses and their conditional cross covariances with system parameters. These covariances are again based on the first-order analysis using the conditional (residual) covariances of parameters from the previous estimate and the sensitivity matrices evaluated with the previously estimated parameter fields (see section 3.3).

[26] **Step 6**. After the new estimate is determined, the residual covariance of the parameter is updated again to reflect the effect of the improvement.

[27] **Step 7**. Repeat steps 4 through 6 until either the successive reduction of the difference between observed and simulated system responses ($\Delta\phi_i$) or successive improvement of the variance of estimated parameter ($\Delta\sigma_{\chi_k}^2$) diminishes to some prescribed value. This iterative algorithm is called the successive linear estimator (SLE), which aims to include the nonlinear relation between the parameter and the response of the system. Convergence of the SLE has been theoretically proved by *Vargas-Guzman and Yeh* [2002].

[28] **Step 8**. The procedures (i.e., Steps 4 through 7) are applied to each data set of all HT tests to derive the final estimate of the hydraulic conductivity field. Following completion of the HT analysis, an analysis of PTT begins and uses the hydraulic conductivity field estimated from HT as the conditional mean field in step 4. Again, Steps 4 through 7 are repeated until data from all PTT tests are exhausted.

[29] Of course, SLE can simultaneously include all the measurements collected from hydraulic and tracer tests during HPTT survey. But we use an efficient way to sequentially add the system responses from HPTT into the estimation process. This approach therefore is called the sequential successive linear estimator (SSLE).

### 3.3. Evaluation of Covariance and Cross Covariance

[30] The covariances of the responses and the cross covariances between the responses and parameters are the heart of the SSLE method. They are evaluated by using a first order analysis as explained below.

[31] Consider that in a system domain discretized into $N$ elements, each element has one value for a given parameter but the value varies from element to element. Suppose that the response of the system is governed by equation (1) or equation (3) and associated boundary and initial conditions. Then, expanding the response at the center of element at $\mathbf{x}_i$ in a Taylor series about the mean value of parameter fields and neglecting second- and higher-order terms, the perturbation of the system responses can be expressed as

$$\varepsilon_\alpha(\mathbf{x}_i, t) \simeq \left. \frac{\partial \phi_\alpha(\mathbf{x}_i, t)}{\partial \ln \chi_k} \right| \zeta_k(\mathbf{x}_j) \tag{11}$$

where $\varepsilon_\alpha(\mathbf{x}_i, t)$ is the perturbation of response $\alpha$ (i.e., head in HT or concentration in PTT) at location $\mathbf{x}_i$ at time $t$; $\zeta_k(\mathbf{x}_j)$ is the perturbation of $\ln \chi_k$ at location $\mathbf{x}_j$, $j$ ranges from 1 to $N$. In the analysis of HT, the subscript $k$ equals 1 and $\ln \chi_k$ represents the log hydraulic conductivity field. In the analysis of tracer tomography, $k$ ranges from 1 to 3. That is, $\ln \chi_1$ represents the log hydraulic conductivity; $\ln \chi_2$ denotes the log water content; $\ln \chi_3$ symbolizes the log DNAPL content. The sensitivity of $\phi_\alpha$ at location $\mathbf{x}_i$ at time $t$ to changes in $\ln \chi_k$ at location $\mathbf{x}_j$ is then specified as $\frac{\partial \phi_\alpha(\mathbf{x}_i, t)}{\partial \ln \chi_k(\mathbf{x}_j)}$. Notice that the Einstein summation convention applies to equation (11) as well as other equations in the paper.

[32] Multiplying equation (11) with a parameter perturbation $\zeta_k(\mathbf{x}_m)$ at a location $\mathbf{x}_m$, and taking the expected value of the product yields the unconditional or conditional cross covariance between the system response, $\varepsilon_\alpha(\mathbf{x}_i)$, and the parameter, $\zeta_k(\mathbf{x}_m)$:

$$R(\varepsilon_\alpha(\mathbf{x}_i, t), \zeta_k(\mathbf{x}_m)) = R(\zeta_k(\mathbf{x}_m), \zeta_k(\mathbf{x}_j)) \frac{\partial \phi_\alpha(\mathbf{x}_i, t)}{\partial \ln \chi_k(\mathbf{x}_j)} \tag{12}$$

where $j = 1, 2, \ldots, N$, $R(\zeta_k(\mathbf{x}_m), \zeta_k(\mathbf{x}_j))$ is the covariance of the parameter $\zeta_k$ between location $\mathbf{x}_m$ and $\mathbf{x}_j$, which is assumed known a priori.

[33] Similarly, assuming the parameters are uncorrelated to each other, the spatial covariance between the system responses at locations $i$ and $m$ is $\varepsilon_i$ and $\varepsilon_m$ given by

$$R(\varepsilon_\alpha(\mathbf{x}_i, t_a), \varepsilon_\alpha(\mathbf{x}_m, t_b)) = R(\zeta_k(\mathbf{x}_p), \zeta_k(\mathbf{x}_q)) \frac{\partial \phi_\alpha(\mathbf{x}_i, t_a)}{\partial \ln \chi_k(\mathbf{x}_p)} \cdot \frac{\partial \phi_\alpha(\mathbf{x}_m, t_b)}{\partial \ln \chi_k(\mathbf{x}_q)} \tag{13}$$

where $p$ and $q = 1, 2, \ldots, N$.

[34] In the case of evaluating the conditional (or residual) covariance and cross covariance, the parameter covariance in equations (12) and (13) is replaced by the conditional covariance of the parameter. The evaluation of the conditional covariance can be found in the work of *Yeh et al.* [1996] and their other publications. Last, the conditional covariance of the estimated parameter approximates the estimation uncertainty due to insufficient information and spatial variability of the parameter.

### 3.4. Evaluation of Sensitivities

[35] The evaluation of covariance and cross covariance requires sensitivities of responses to the changes in parameters. The popular adjoint state method [e.g., *Sykes et al.*, 1985; *Sun*, 1994] is adopted to evaluate the sensitivities of responses to parameters. A brief summary of the derivation of the sensitivity of tracer concentration to parameters is given below. The derivation of the sensitivity required for

HT analysis is available in the works of *Yeh and Liu* [2000] and *Zhu and Yeh* [2005].

[36] Given a set of concentration measurements during one tracer test, the adjoint state method first solves for mean heads and concentrations throughout the domain using equations (1) and (3) with associated boundary and initial conditions. Next, for each concentration measurement, two adjoint states, $\psi_c$ and $\psi_h$, are derived for concentration and head, respectively, through solving the following adjoint state equations [*Sun*, 1994; *Li and Yeh*, 1999]:

$$-\nabla\cdot(\psi_c\bar{\mathbf{q}})-\nabla\cdot\left(\bar{\theta}_w\mathbf{D}\nabla\psi_c\right)-\left(\bar{\theta}_w+\bar{\theta}_nK_N\right)\frac{\partial\psi_c}{\partial t}+\frac{\partial R}{\partial c}=0 \tag{14}$$

$$\nabla\cdot(\bar{K}\nabla\psi_h)+\nabla\cdot(\bar{K}\psi_c\nabla\bar{c})+\frac{\partial R}{\partial H}=0 \tag{15}$$

subject to the boundary and final time conditions:

$$\begin{aligned}
\psi_c &= 0 && \text{at } \Gamma_1\\
\bar{q}_i\psi_c+D_{ij}\frac{\partial\psi_c}{\partial x_j} &= 0 && \text{at } \Gamma_2\\
\psi_h &= 0 && \text{at } \Gamma_1\\
-\bar{K}\frac{\partial\psi_h}{\partial x_j} &= \psi_c\bar{K}\frac{\partial\bar{c}}{\partial x_j} && \text{at } \Gamma_2\\
\psi_c|_{t=T_e} &= 0
\end{aligned} \tag{16}$$

where the overhead denotes the mean; $R = c\delta(x - x_k)(t - t_l)$ represents the concentration measurement at location $x_k$ and time $t_l$, where $\delta$ is Dirac delta function, which equals unity if $x$ equals $x_k$ and $t$ equals $t_l$, 0 otherwise. The evaluation of the adjoint state $\psi_c$ at a given observation location is obtained by solving equations (14) only once for the last observation time regardless of the number of observations in time (a suggestion from Tom Clemo, Boise State University). Using $\frac{\partial\chi(\mathbf{x}_n)}{\partial\ln\chi(\mathbf{x}_n)}=\chi(\mathbf{x}_n)$, the sensitivity of tracer concentration at location $x_k$ and time $t_l$ to parameters at location $\mathbf{x}_n$ are given by:

$$\frac{\partial c(\mathbf{x}_k,t_l)}{\partial\ln K(\mathbf{x}_n)}=\int_T\int_{\Omega_n}\left[-\bar{K}\nabla\psi_h\nabla\bar{H}-\psi_c\bar{K}\nabla\bar{c}\nabla\bar{H}\right]\mathrm{d}\Omega\mathrm{d}t \tag{17}$$

$$\frac{\partial c(\mathbf{x}_k,t_l)}{\partial\ln\theta_w(\mathbf{x}_n)}=\int_T\int_{\Omega_n}\left[\bar{\theta}_w\nabla\psi_c\mathbf{D}\nabla\bar{c}+\bar{\theta}_w\psi_c\frac{\partial\bar{c}}{\partial t}\right]d\Omega dt \tag{18}$$

$$\frac{\partial c(\mathbf{x}_k,t_l)}{\partial\ln\theta_n(\mathbf{x}_n)}=\int_T\int_{\Omega_n}K_N\bar{\theta}_n\psi_c\frac{\partial\bar{c}}{\partial t}d\Omega dt \tag{19}$$

where $\Omega_n$ is the volume of the element where the observation location $\mathbf{x}_n$ belongs. In our formulation of the adjoint methods, we assume the tracer transport induced by a tracer test is advection-dominated, and the local dispersion coefficient is known and constant. A more comprehensive formulation of the adjoint equations is given by *Sun and Yeh* [1990].

## 4. Numerical Experiments

### 4.1. Mathematical Validation of the Estimator

[37] Before investigating the effectiveness of HPTT, we validated the SSLE using a mathematically well-posed problem in a test bed. The test bed is a one-dimensional horizontal aquifer which is 40 m long and discretized into 40 elements with uniform size of 1.0 m. The initial condition for the hydraulic head field is 100 m and 0 tracer concentration everywhere. The head value was used as the prescribed head boundary conditions at the two ends of the aquifer, whereas 0 concentration gradients are used as boundary conditions for the solute transport equation. Using the spectral method by *Gutjahr* [1989], we generated lognormally distributed $K$, $\theta_w$, and $\theta_N$ fields with the following spatial statistics. The geometric means of the $K$, $\theta_w$, and $\theta_N$ fields are 0.62 m/d, 0.35, and 0.15, respectively, and the variances of the natural logarithm of the three fields are 0.477, 0.030, and 0.096, respectively. These three fields have the same exponential correlation structure with a correlation scale of 10 m. The longitudinal and transverse dispersivities were set to be constant throughout the domain, with a value of 0.05 and 0.01 m, respectively. The molecular diffusivity was set to $10^{-7}$ m$^2$/d for each element.

[38] A forward simulation of a partitioning tracer test was conducted subsequently. Specifically, we simulated a steady flow field in the aquifer caused by a continuous injection of water into the center of the aquifer ($x$ = 19.5 m) at the rate of 0.5 m$^3$/d. Next, on the basis of the flow field, simulations of the migration of a slug of conservative and partitioning tracers were carried out for a period of 45 days. The slugs of tracers were released at a concentration of 1 kg/m$^3$ over a period of 10 days at the injection location. During the simulation of the transport of the conservative tracer, the partitioning coefficient in equation (3) was set to 0 such that the generated $\theta_w$ field was the pore space through which the tracer migrated. Then, the coefficient was set to 3.0 and the generated $\theta_w$ and $\theta_N$ fields were fully specified to simulate BTCs of the partitioning tracer at the sampling locations.

[39] Upon completion of the forward simulations, the steady state head value at each element and one of the conservative and partitioning tracer BTC data at all the 40 elements were regarded as available information for the inverse modeling, as were the $K$, $\theta_w$, and $\theta_N$ values at the left end of the aquifer. In addition, the dispersivity and the diffusivity were presumed to be known. All these pieces of information are the necessary and sufficient conditions for the inverse problem to be mathematically well posed. Our stochastic estimator or any inverse model, if its algorithm is correct, should yield exact estimates or estimates close to the true values of the generated $K$, $\theta_w$, and $\theta_N$ fields.

[40] To carry out the validation, we first used the hydraulic head data to estimate the $K$ field. Then, treating the estimated $K$ field as a given hydraulic property of the aquifer, we made use of the conservative tracer measurements to estimate the $\theta_w$ field. With these estimated $K$ and

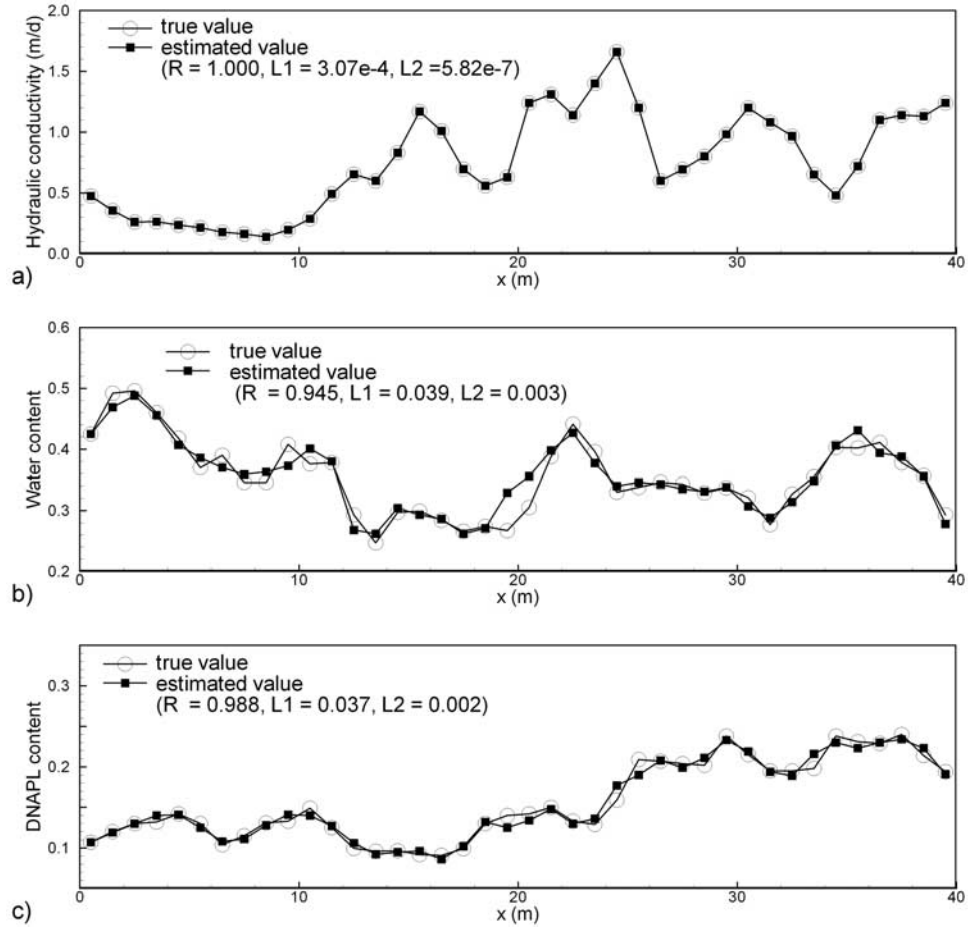


**Figure 1.** Comparisons of the estimated and true hydraulic conductivity, water content, and DNAPL content fields for a well-posed problem.

$\theta_w$ fields as fully specified information, estimation of $\theta_N$ distribution then followed using the partitioning tracer measurements.

[41] Performances of our estimator were evaluated using the correlation value, mean absolute error norm $L1$, and mean square error $L2$. The correlation between log-transformed true and estimated field, $\chi_i$ and $\hat{\chi}_i$, respectively, is calculated from

$$R = \frac{\frac{1}{N}\sum_{i=1}^{N}(\chi_i - \mu_\chi)(\hat{\chi}_i - \mu_{\hat{\chi}})}{\sqrt{\frac{1}{N}\sum_{i=1}^{N}(\chi_i - \mu_\chi)^2 \cdot \frac{1}{N}\sum_{i=1}^{N}(\hat{\chi}_i - \mu_{\hat{\chi}})^2}} \quad (20)$$

where $N$ is the total number of elements. $\mu_\chi$ and $\mu_{\hat{\chi}}$ are means for true and estimated value, respectively. $L1$ and $L2$ are calculated using

$$L1 = \frac{1}{N}\sum_{i=1}^{n}|\chi_i - \hat{\chi}_i| \quad \text{and} \quad L2 = \frac{1}{N}\sum_{i=1}^{n}(\chi_i - \hat{\chi}_i)^2 \quad (21)$$

[42] The validation results are illustrated in Figure 1, which shows the estimated and true $K$, $\theta_w$, and $\theta_N$ fields, and lists the correlation values between the estimated and true fields. According to the correlation values and plots, results of the validation are deemed satisfactory; the joint estimator yields estimates of all the parameter fields in a close agreement with the true field under well-posed situations. Lower correlation and greater $L1$ and $L2$ values are expected for $\theta_w$ and $\theta_N$ estimates because of greater numerical errors in solving the governing equations as well as the adjoint equations associated with $\theta_w$ and $\theta_N$. We thus conclude that our stochastic estimator algorithm is mathematically valid.

### 4.2. Importance of Hydraulic Heterogeneity

[43] Following the validation, we used four hypothetical scenarios based on the setup of the previous one-dimensional test bed to investigate impacts of prior knowledge of the spatial distribution of $K$ and $\theta_w$ on the estimation of $\theta_N$. To estimate the $\theta_N$ distribution for all the cases, one concentration of the rising limb of the simulated partitioning tracer BTCs at all 40 elements were employed. The first case is identical to the well-posed problem in the validation section. That is, the true $K$ and $\theta_w$ fields are known precisely except the $\theta_N$ field. Case 2 represents the situation in which the $\theta_N$ field is unknown but the true $K$ field is given, and the $\theta_w$ field is incorrectly assumed to be uniform with a value equal to the mean of its true field. In case 3, the true $\theta_w$ field

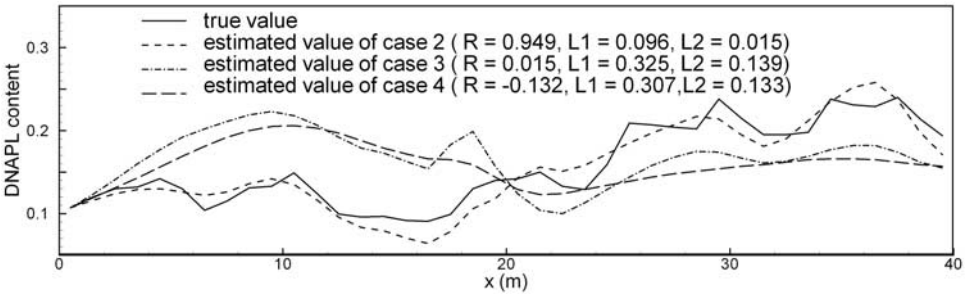


**Figure 2.** Estimated DNAPL in one-dimensional problem using partitioning tracer BTCs; case 2, the true $K$ field is fully specified but the $\theta_w$ field is given using its mean value; case 3, the $K$ field is specified using its mean value and the true $\theta_w$ field is fully specified; case 4, both the mean of true $K$ and $\theta_w$ fields were used as the true field.

is known, and the $K$ field is falsely regarded as homogeneous with a value equal to the mean of the true field. Last, both $K$ and $\theta_w$ fields are incorrectly assumed to be constants equal to the mean values of their true fields (case 4).

[44] Figure 2 shows estimated $\theta_N$ fields of cases 2, 3, and 4 as well as the true $\theta_N$ fields; the estimated fields for case 1 are given in Figure 1c. The correlation value between the true and the estimate for each case is also reported in the figure. A comparison of the estimated $\theta_N$ fields in case 1 (known true $K$ and $\theta_w$ fields) and case 2 (known true $K$ field but only mean $\theta_w$ field) indicates that an exact knowledge of the $\theta_w$ field slightly improves estimation of the detailed $\theta_N$ distribution. In contrast, a comparison of the results from cases 1 and 2 (the true $K$ field known) and from cases 3 and 4 (the true $K$ field unknown) reveals that the knowledge of the exact $K$ field significantly impacts the general pattern of the estimated $\theta_N$ distribution. The correlation values for cases 3 and 4 are small and negative, indicating an opposite trend of the estimated $\theta_N$ distribution in comparison with the true. These results corroborate our hypothesis presented in the introduction section about the importance of site characterization prior to or during any partitioning tracer test.

### 4.3. Advantages of Tomographic Surveys

[45] In section 4.2, we demonstrated that for successfully mapping the $\theta_N$ distribution, a complete knowledge of hydraulic heterogeneity is critical. HT is a viable technology to obtain this knowledge. Inasmuch as the usefulness of HT for the characterization of the hydraulic conductivity and specific storage fields has been documented by *Zhu and Yeh* [2005] and *Liu et al.* [2007], we used here the one-dimensional test bed to investigate the benefit of PTT over a single tracer test. To facilitate this, the $K$ field is assumed to be known precisely (in turn, the specific discharge or the Darcy velocity field). Instead of collecting BTCs at every element of the aquifer as in section 4.1, here we collect them from only nine monitoring points at $x$ = 3.5, 7.5, 11.5, 15.5, 19.5, 23.5, 27.5, 31.5, and 35.5 m. This scenario represents a mathematically ill-posed inverse problem for identifying $\theta_w$ and $\theta_N$ distributions due to insufficient information. Three sequential tracer tests were simulated at $x$ = 7.5, 19.5, and 31.5 m independently. Before each tracer test, water was injected at the injection location to reach a steady state. Then, a slug of a conservative and a partitioning tracer was released over a period of 10 days. Each test was simulated for 100 days to obtain complete BTCs at the eight wells (excluding the injection well). For this investigation, we examined the following effects of two sampling strategies on the estimation of the $\theta_w$ and $\theta_N$ distribution: (1) only one conservative and partitioning tracer concentration at early part of the rising limb of the BTCs, and (2) three concentration values at three different times of the BTCs.

[46] The true and estimated $\theta_w$ and $\theta_N$ fields based on one, two, and three tracer tests with the first sampling strategy are plotted in Figures 3a and 3b, respectively. The corresponding correlations between the true and the estimated $\theta_w$ as well as those of the $\theta_N$ fields are also listed in the figures. These plots and correlation values indicate that with the perfectly known flow field, the PTT (i.e., two or three tracer tests) improves the estimation of the detailed $\theta_w$ and $\theta_N$ distributions but the improvement diminishes as the number of tests increases to three.

[47] Results of the second sampling strategy are shown in Figures 4a and 4b. A comparison of Figures 3a and 3b and Figures 4a and 4b as well as their correlation values suggests that more frequent samples in time of the BTCs can improve the estimate of both $\theta_w$ and $\theta_N$ distributions. This finding reflects the fact that a BTC is a time record of tracer particles arriving at the sampling port via various flow paths. Each concentration measurement bears information about a solute travel path.

[48] On the basis of these results, our hypothesis thus is corroborated that tracer tomographic surveys can provide more detailed mapping of the $\theta_N$ distribution than the traditional interwell partitioning tracer test when the $K$ field is known.

### 4.4. Advantages of the Proposed HPTT in a Multidimensional Aquifer

[49] To further test effectiveness of the HPTT concept and our estimator for mapping DNAPLs, we applied the HPTT technology to a quasi three-dimensional (or two-dimensional), hypothetical, heterogeneous aquifer, which was assumed to be contaminated with a single component DNAPL. This aquifer was 40 m long in horizontal direction, 0.5 m in width, and 10 m deep in the vertical direction. A fixed head of 100 m was specified at the left-hand and the right-hand boundaries whereas no flow was specified at other boundaries. The aquifer was discretized into 1600 elements with a uniform element size of 0.5 × 0.5 × 0.5 m.

[50] Spatial distributions of $K$, $\theta$, and $\theta_N$ in the aquifer (Figures 5a, 7a, and 9a, respectively) were generated by the

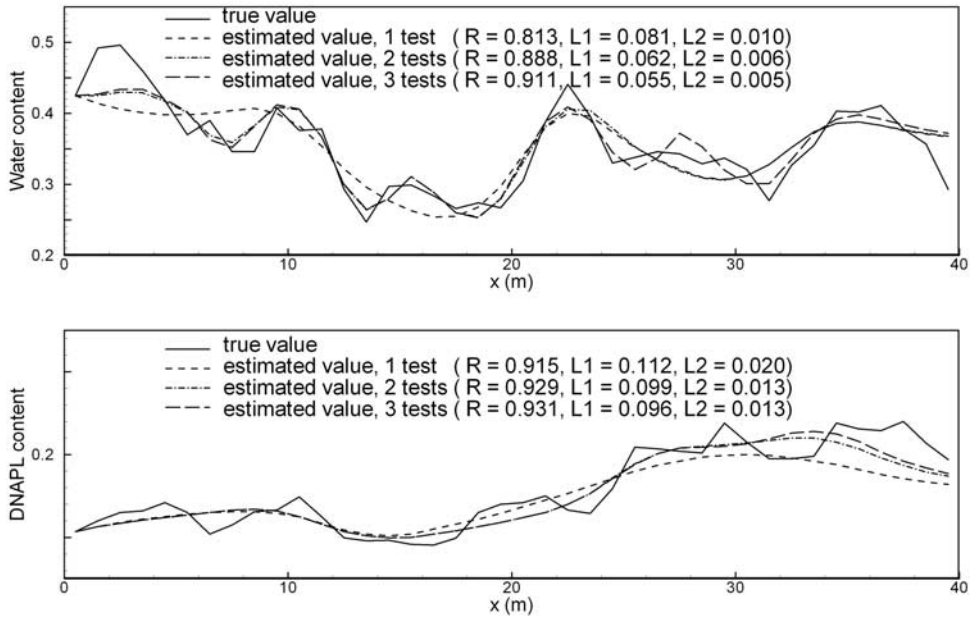


**Figure 3.** Comparison of the true and estimated (a) $\theta_w$ or (b) $\theta_N$ field using one concentration measurement of each BTC during the conservative and partitioning tracer tomography with the assumption that the true $K$ field is known.

spectral method. They all were assumed to be lognormal distributed and uncorrelated with each other. The $K$ field was generated with a geometric mean of 0.86 m/d with a variance of 1.68 (0.8 for ln $K$). The porosity ($\theta$) of the aquifer had a geometric mean of 0.4 and a variance of 0.0033 (0.02 for ln $\theta$). Similarly, the $\theta_N$ field was created with a geometric mean of 0.1 and a variance of 0.012 (0.1 for ln $\theta_N$). The $\theta_w$ field was then obtained by subtracting $\theta_N$ from the generated $\theta$ field. The geometric mean of the resultant $\theta_w$ field was 0.291, and the variance was 0.004 (0.057 for ln $\theta_w$). We assumed that an exponential correlation function characterized the spatial statistical structures of the three fields, with a horizontal correlation scale of 3.5 m and a vertical correlation scale of 1.5 m. We further assumed that the spread of the tracer was dominated by velocity variations caused by the heterogeneous $K$ and $\theta_w$ fields. Therefore, throughout the domain, the longitudinal and transverse dispersivities were set to be constant as 0.05 and 0.01 m, respectively. The molecular diffusivity was set as $10^{-7}$ m$^2$/d everywhere. The values of these parameters

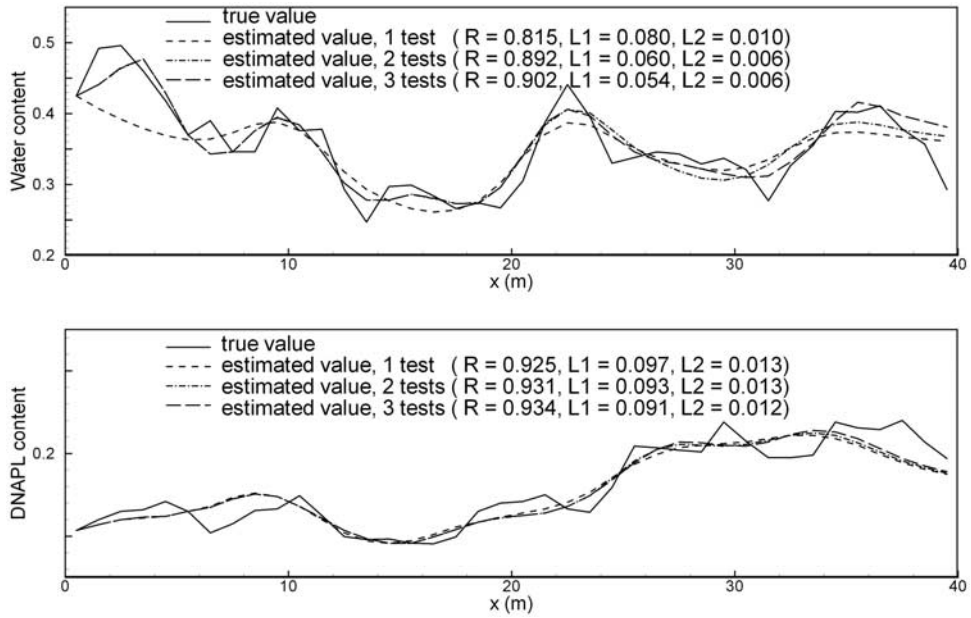


**Figure 4.** Comparison of the true and estimated (a) $\theta_w$ or (b) $\theta_N$ field, using three concentration measurements of each BTC during the conservative and partitioning tracer tomography with the assumption that the true $K$ field is known.

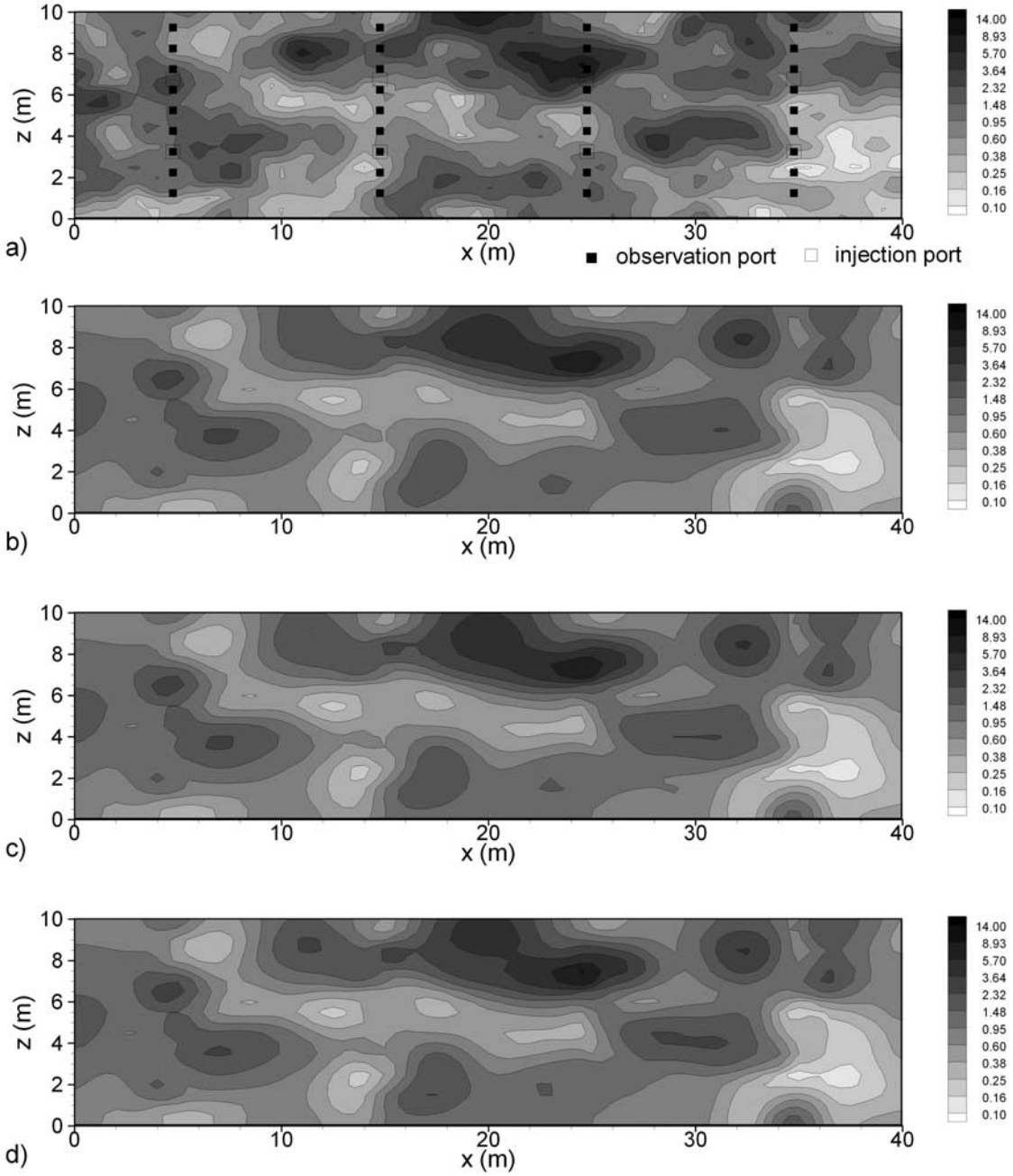


**Figure 5.** Comparison between true and estimated $K$ field: (a) true field; (b) estimate using head data only; (c) estimate using head and conservative data; (d) estimate using head, conservative tracer, and partitioning tracer data.

were presumed to be determined prior to the analysis of HPTT. The partitioning coefficient of the partitioning tracer was assumed to have a value of 9.0, which corresponds to the TCE partitioning coefficient value of a 4-mehtyl-2-pentanol tracer [*Dugan et al.*, 2003].

[51] To conduct HPTT in this synthetic aquifer, four fully penetrating wells were emplaced in the aquifer. Each well had nine pressure and tracer dual-purpose sampling ports and two injecting ports (Figure 5a). The distance between any pair of the wells was 10 m, about 2.86 times longer than horizontal correlation scale. This well field design was based on the suggestion by *Yeh and Liu* [2000] that the ''optimum'' distance between wells for hydraulic tomography is one correlation scale of the hydraulic property. $K$, $\theta_w$, and $\theta_N$ values were sampled in all the 36 monitoring ports and used as our prior information. Mean, correlation scales and variances of three variables were then estimated using the samples, and they were later used in the SSLE.

[52] Eight tracer injections at the four wells were simulated subsequently. Prior to each tracer injection, a steady state flow field was simulated, resulting from a continuous injection of water into the aquifer at a rate of 20 $m^3$/d through one of the eight injection ports. Using the steady state flow field, migration of a slug of conservative and partitioning tracers of 1 kg/$m^3$ was then calculated, each being released at the same port into the aquifer for 0.9 days.

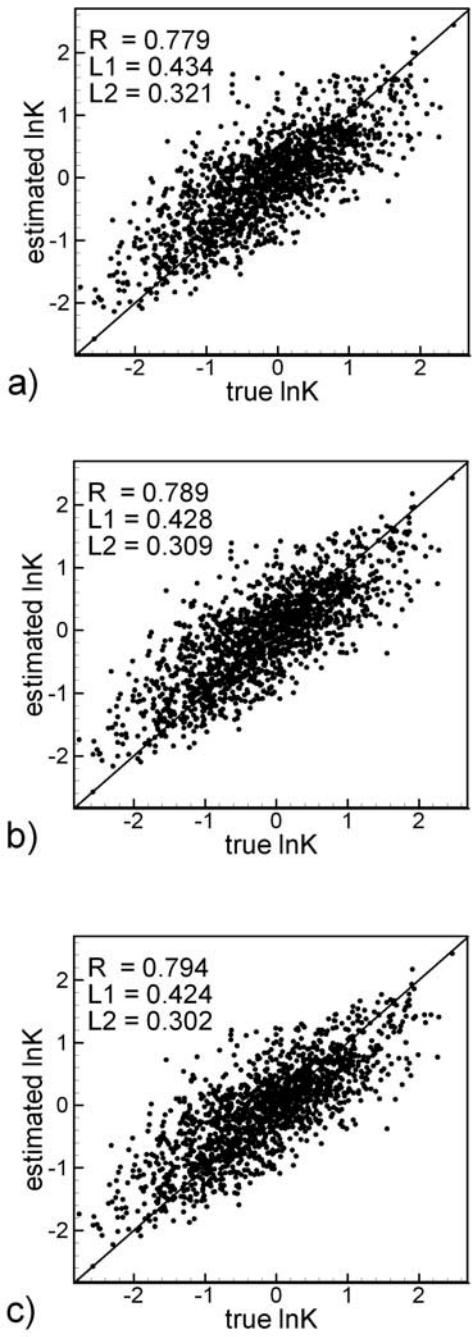


**Figure 6.** Scatterplot of true $K$ field versus the estimated from (a) head data, (b) head and conservative tracer data, (c) head, conservative tracer, and partitioning tracer data.

The simulation was carried out for a period of 12 days during which both conservative and partitioning tracer breakthroughs were recorded at all the observation ports at all wells (except the injection port). Nine concentration measurements for each complete BTC were selected for the estimation (four near equally distributed measurements of the rising limb, one at the peak, and four at the falling limb). For those sampling ports where only a portion of a breakthrough was recorded during the 12-day period, a smaller number of samples were collected but the same sampling strategy was used. The steady state heads at these observation ports were also recorded during each test. For the eight tests, 288 steady state head measurements, 2192 conservative tracer concentration measurements, and 1659 partitioning tracer concentration measurements were collected, and we refer to them as secondary information.

[53] The prior information and the secondary information were then applied to three scenarios to illustrate the advantage of the joint HT and PTT. First, we considered a scenario in which neither the $K$ field nor the $\theta_w$ field were known before hand, except for the $K$, $\theta_w$, $\theta_N$ values obtained from the 36 monitoring ports. All of the data sets from the HPTT survey were utilized to map the $\theta_N$ distribution. The estimation commenced with the use of the head information from HT to estimate the $K$ field. Then, in conjunction with the previously estimated $K$ field from HT, we took advantage of the conservative tracer data from PTT to simultaneously estimate the $\theta_w$ field and improve the estimation of the $K$ field. The estimation of the $\theta_N$ distribution then followed using the partitioning tracer test data. During this step, the previously estimated $K$ field and $\theta_w$ field from head and conservative tracer data were regarded as our prior knowledge of the aquifer. The SSLE was then used to analyze the partitioning tracer data to estimate the $\theta_N$ distribution and to improve the estimate of $K$. Note that the previously estimated $\theta_w$ field was fixed without any update. While this case tests the effectiveness of HPTT and the estimator under a more realistic scenario, it also served the purpose of evaluating improvement of the $K$ estimates from HT due to inclusion of observed tracer concentration data from the tracer tomography. Eight nodes (Pentium 2.8 GHz each) of a PC cluster were used for this experiment. The total CPU runtime was about 425 min, including 25 min for inverting head information, 200 min for inverting conservative tracer data, and 200 min for inverting partitioning tracer data.

[54] For the second scenario, we investigated the effectiveness of a traditional partitioning tracer test similar to that used by *Jin et al.* [1995]. Specifically, previously simulated concentration measurements at all of the sampling ports due to one tracer injection at a location ($x$ = 14.75 m, $z$ = 6.75 m) were employed to estimate the DNAPL distribution. Different from the work of *Jin et al.* [1995], we estimated the $\theta_w$ field in addition to the $K$ and $\theta_N$ fields.

[55] Finally, we investigated the effectiveness of a traditional borehole sampling approach (scenario 3). In other words, using the measured DNAPL content at the 36 observation points, we used the kriging method to estimate DNAPL distribution of the entire aquifer. An exponential variogram model was used with a sill of 0.1, horizontal range 3.5 m, vertical range 1.5 m. This variogram was the one used to generate the synthetic $\theta_N$ field.

[56] Results of these experiments are discussed as follows. Effectiveness for mapping the $K$ field using hydraulic head measurements and data of a conservative and a partitioning tracer during the HPTT is demonstrated in Figures 5 and 6. Figure 5a shows the true distribution of the $K$ field while the estimated field using the steady hydraulic head information of HT is plotted in Figure 5b. Figure 5c depicts the estimated $K$ field on the basis of both head and conservative tracer concentration data from the HPTT. Last, the estimated $K$ field shown in Figure 5d represents the estimate using all the head, conservative

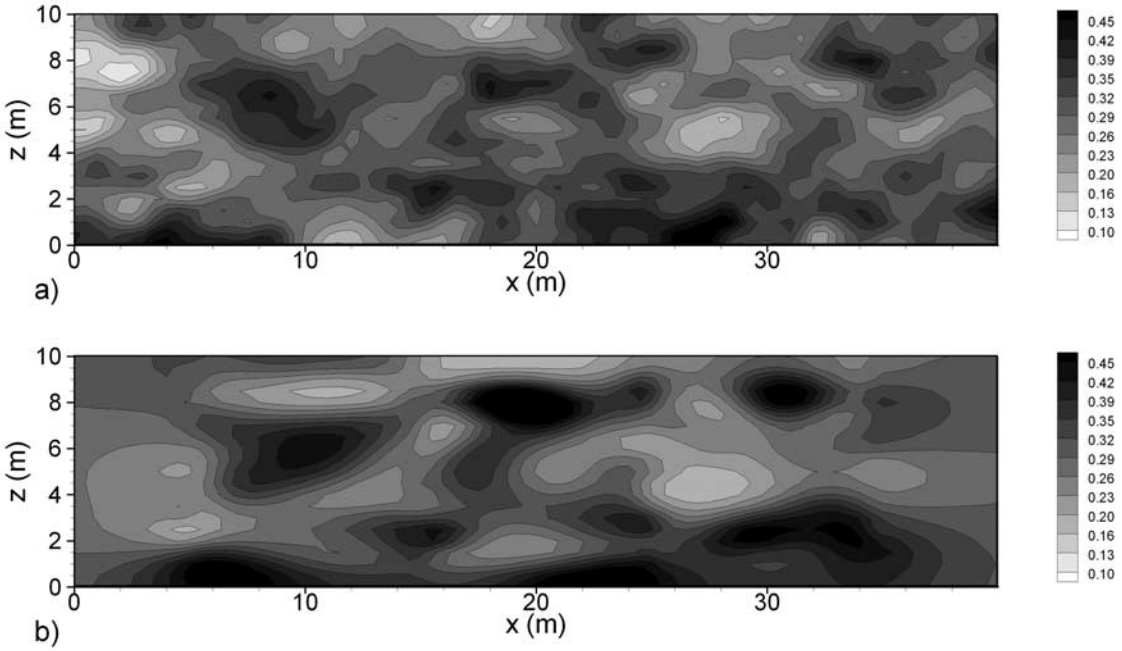


**Figure 7.** Comparison between estimated $\theta_w$ field and true field. (a) True field; (b) estimate using conservative tracer data.

tracer, and partitioning tracer measurements during the HPTT. The scatterplots and correlations, $L1$, and $L2$ norms corresponding to the three scenarios (Figures 5b, 5c, and 5d) are given in Figures 6a, 6b, and 6c, respectively. Both the plots and the quantitative measures indicate that the estimate based on head data alone already is close to the true $K$ field. Inclusion of the data of conservative tracer improves the estimate, and additional partitioning tracer data further enhance it but very slightly. This finding about the relative worth of different types of data is consistent with the finding reported by *Li and Yeh* [1999].

[57] Results of estimation of the $\theta_w$ field using the conservative data are shown Figures 7 and 8. A comparison of Figure 7a (the true $\theta_w$ field) with Figure 7b (the estimated) suggests that the conservative tracer data from HPTT captures the general pattern of the true $\theta_w$ distribution. However, the estimated field apparently has higher $\theta_w$ values than the true around the locations where the true $\theta_w$ are high. A scatterplot of the estimated and true field as well as the three quantitative measures is shown in Figure 8. This figure shows that our estimated $\theta_w$ field is unbiased with relatively large scattering. Notice that we used the estimated $K$ field from head data as our prior knowledge to estimate $\theta_w$.

[58] In regard to the primary objective of HPTT (i.e., estimation of $\theta_N$ distribution), estimated $\theta_N$ distributions from the above three scenarios are illustrated in Figure 9. Figure 9b shows the estimated $\theta_N$ field based on the HPTT approach; we used the estimated $K$ and $\theta_w$ fields from head and conservative tracer data of HPTT as our prior information and then used the partitioning tracer data to simultaneously estimate the $\theta_N$ and $K$ distributions while the prior $\theta_w$ field was fixed. According to the figure, our approach identifies the patterns of the true DNAPL distribution (Figure 9a) satisfactorily. However, the presences of DNAPL near the boundaries of the domain are not identified. Poor estimation near the left and right boundaries can be attributed to the fact that no sampling ports were placed at the boundary to intercept the partitioning tracer. The underestimation of DNAPL near the upper and lower boundaries is caused by migration of the partitioning tracer parallel to the boundaries. The partitioning tracer, as such, was undetected by the uppermost and lowest sampling ports.

[59] Figure 9c illustrates the estimated $\theta_N$ field based on only BTCs data at all of the sampling ports during one tracer injection test (traditional partitioning tracer test). The resultant estimate apparently is smoother and inferior to that in Figure 9b, where HPTT was used. This can be attributed to the fact that HPTT provides more information to constrain the estimation.

[60] Finally, the estimated $\theta_N$ distribution based on kriging and the 36 samples is plotted in Figure 9d. In comparison with the results from the other approaches (Figure 9 and 9c),

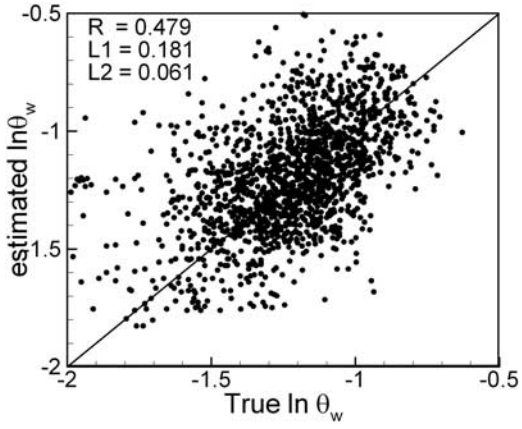


**Figure 8.** Scatterplot of estimated water content field versus true field.

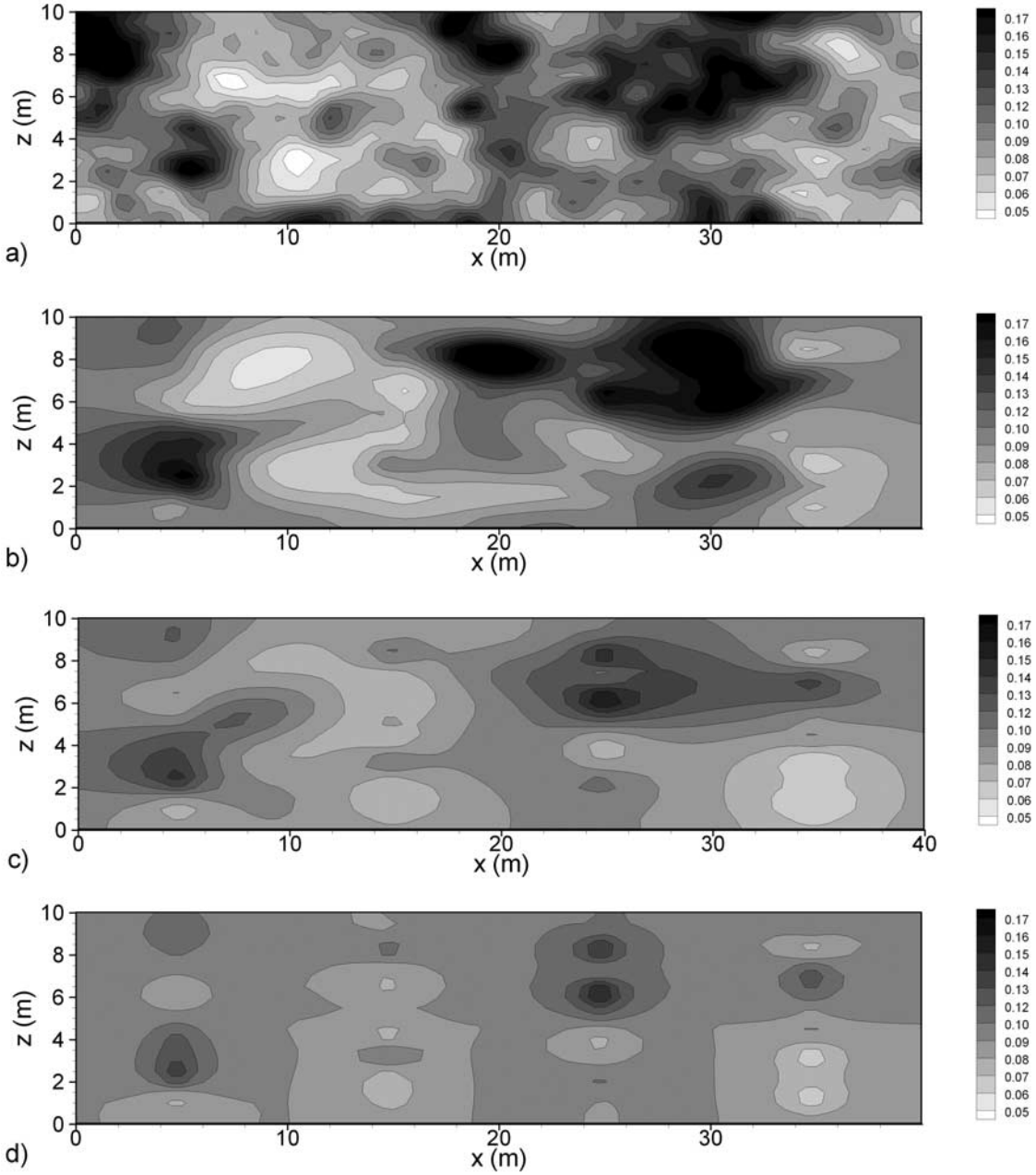


**Figure 9.** Comparison between true and estimated DNAPL content field. (a) true field; (b) estimate from hydraulic/tracer tomography; (c) estimate from a single tracer test; (d) estimate from kriging using the 36 samples.

the direct sampling approach yields the smoothest estimate. It detects DNAPL near sampling locations and extrapolated the sample values to its vicinity via the correlation structure but fails to capture high $\theta_N$ areas between observation wells. The scatterplots as well as the three quantitative measures (correlation, $L1$, and $L2$ norms) for the results shown in Figures 9b, 9c, and 9d are illustrated in Figures 10a, 10b, and 10c, respectively, confirming our findings quantitatively. The volumes of DNAPL estimated by the three approaches are tabulated in Table 1. The result also indicates that HPTT yielded a closer estimate of the volume of DNPL to the true than the other two approaches.

[61] For the numerical examples reported here, the maximum number of iterations required is 20, which is partially attributed to the continuous update of the residual covariance of the parameters as well as the convergence criterion of SSLE. Two criteria are used in SSLE, the difference in the variance of the estimated parameter field at two successive iterations and the change in difference between the observed and simulated system responses at two successive iterations.

## 5. Discussion and Conclusions

[62] The SSLE developed for HPTT to characterize DNAPL source zones in the subsurface was satisfactorily validated using a well-posed numerical example. Numerical experiments using the SSLE subsequently demonstrate that knowledge of the true hydraulic conductivity distribution

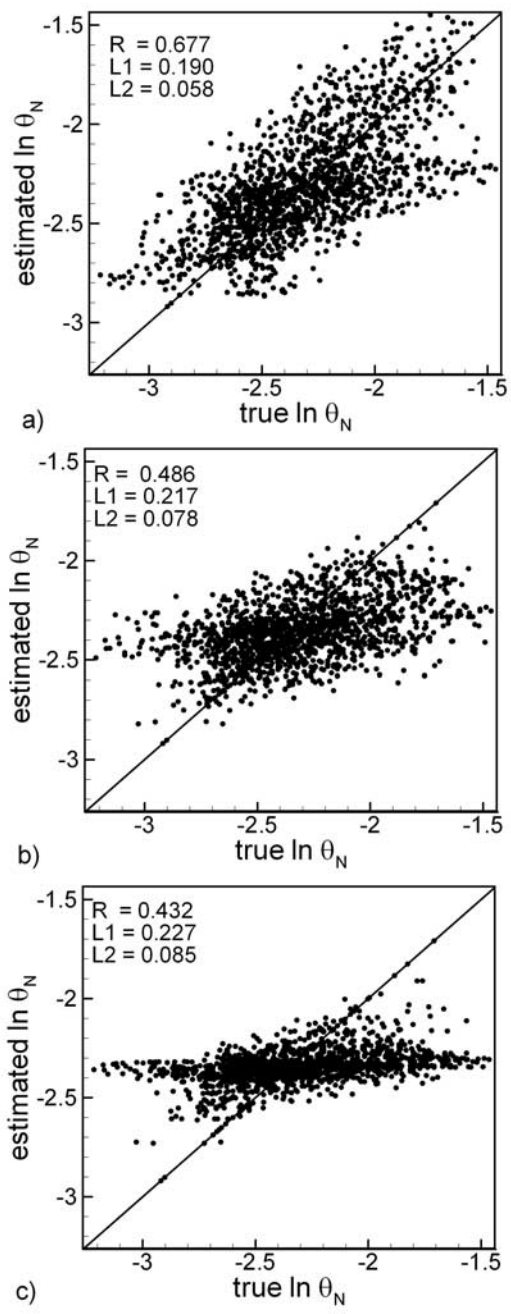


**Figure 10.** Scatterplot of true DNAPL content field versus the estimated field from (a) hydraulic/tracer tomography, (b) single tracer test, (c) kriging using the 36 samples.

plays a more important role than the true water content in the analysis of a partitioning tracer test to detect the DNAPL distribution in aquifers. If the heterogeneous hydraulic conductivity field is known precisely, a single dual tracer test can yield the general pattern of the DNAPL distribution. But PTT can reveal more details if only a limited number of tracer sampling locations are available. The resolution of the distribution can be further enhanced if frequently sampled concentration data of tracer breakthroughs are available.

[63] Results of the experiments with a multidimensional aquifer show that additional tracer data from PTT improve the $K$ estimates based on HT only but very slightly. The head information brings forth the major pattern of spatial variation of the $K$. Similar findings were also reported by *Li and Yeh* [1999] and *Cirpka and Kitanidis* [2001]. Results of the experiments also confirm that our proposed HPTT can reveal more detailed DNAPL distribution than the conventional single dual tracer test that does not exploit the hydraulic head information or prior characterization of the hydraulic conductivity field. The kriging method using in situ point samples of DNAPLs on the other hand produces the smoothest estimates among the other approaches.

[64] Although not shown in this paper, the experiments also indicate that PTT alone, i.e., without taking advantage of the hydraulic head information, can lead to erroneous estimates of the DNAPL field. This finding can be attributed to the fact the tracer data from one injection test provide only an estimate of the Darcy velocity (specific discharge) field for the given flow scenario, which is only weakly related to the $K$ field unless the hydraulic head or gradient field is specified. While PTT can produce many sets of estimated Darcy velocity fields, each field is weakly related to the others. That is, the velocity fields are a function of not only a site-specific hydraulic conductivity field but also the head or gradient fields corresponding to different injections. Without conditioning the estimation using the available head information of all the injections, information of one velocity field does not constrain the other velocity fields. The estimation of DNAPL distribution thus remains poorly posed, and the estimates can be worsened. Consequently, without detailed characterization of the $K$ field in a source zone, it is difficult to obtain a realistic map of DNAPL distribution. Likewise, an effective remediation also depends upon the characterization of the hydraulic conductivity field. A conjunctive use of HT and PTT is therefore a logical approach for better DNAPL characterization.

[65] On the basis of the results of this study, we recommend that during a HPTT test, the usefulness of HT should be maximized to characterize the hydraulic heterogeneity in detail. Afterward, PTT that involves two dual tracer tests is deemed sufficient to estimate DNAPL distributions. During PTT, the breakthrough concentration should be sampled as frequently as possible to enhance the DNAPL estimates. Likewise, an increase of the number of PTT tests would increase the resolution of the DNAPL estimates but at greater costs.

[66] We must emphasize that this study is merely a proof of concept. Field situations undoubtedly are more complicated than the synthetic cases. A workable technology for field applications remains to be developed. Several assumptions embedded in this study and some possible complications in the field are discussed below, as well as some limitations of the SSLE algorithm.

**Table 1.** The Volume of Dense Nonaqueous Phase Liquid (DNAPL) Estimated by the Three Approaches

| | | Total DNAPL Volume | | |
|---|---|---|---|---|
| | | Estimated DNAPL | | |
| | True | HPTT | Single Tracer Test | Kriging |
| Volume | 21.033 | 20.817 | 19.340 | 19.279 |
| Variance | 0.1 | 0.076 | 0.024 | 0.008 |

[67] First, the current partitioning tracer technology assumes that partitioning tracers react only with DNAPLs. Partitioning tracers can actually react with many unknown organic matters in the field. This assumption thereby may lead to false identification of the presence of DNAPLs. In addition, it is likely that nonideal partitioning processes between the tracers and DNAPLs exist in the field. This will certainly complicate the analysis of traditional partitioning tracer tests as well as that of HPTT. The equilibrium partition assumption, we believe, nevertheless is sufficient for identifying the general distribution of DNAPLs in the field.

[68] The assumption of immobilization of DNAPLs caused by the injections in existing partitioning tracer technology and the HPTT may limit their applications to sites containing residual DNAPLs only. This concern may be minimized by adopting a multiphase modeling approach for the analysis. A multiphase model nevertheless adds additional challenges and uncertainty in the analysis of partitioning tracer tests.

[69] Last, the major barrier of the SSLE algorithm for a large-scale problem (e.g., millions of nodes) is the memory requirement for storing the residual covariance of each parameter field to be estimated since SSLE propagates and updates these covariances during iterations and between HT and PTT. This issue is currently being investigated. It is also worthwhile to emphasize the fact that the SSLE has been applied to HT experiments in sandboxes, which involve possible measurement and model errors (*Liu et al.*, 2002, 2007), and these applications have demonstrated that the SSLE yields satisfactory results.

[70] **Acknowledgments.** The work reported is a part of a collaborative research with Walter Illman at University of Iowa, who is conducting sandbox validation of HPTT, and the research is primarily supported by a SERDP grant subcontracted through the University of Iowa, and in part by NSF grant EAR-0229717, NSF IIS-0431079, and NSF EAR-0450388. We express our gratitude to our collaborator, Water Illman, for valuable comments and suggestions on the idea of HPTT, as well as discussions of partitioning tracers with William Blanford at Louisiana State University at the early stage of the project. We also gratefully acknowledge Martha P. L. Whitaker for the technical editing of this manuscript.

## References

Beckie, R., and C. F. Harvey (2002), What does a slug test measure: An investigation of instrument response and the effects of heterogeneity, *Water Resour. Res.*, *38*(12), 1290, doi:10.1029/2001WR001072.

Bohling, G. C., X. Zhan, J. J. Butler Jr., and L. Zheng (2002), Steady shape analysis of tomographic pumping tests for characterization of aquifer heterogeneities, *Water Resour. Res.*, *38*(12), 1324, doi:10.1029/2001WR001176.

Brauchler, R., R. Liedl, and P. Dietrich (2003), A travel time based hydraulic tomographic approach, *Water Resour. Res.*, *39*(12), 1370, doi:10.1029/2003WR002262.

Cirpka, O. A., and P. K. Kitanidis (2001), Sensitivity of temporal moments calculated by the adjoint-state method and joint inversing of head and tracer data, *Adv. Water Resour.*, *24*(1), 89–103.

Datta-Gupta, A., S. Yoon, D. W. Vasco, and G. A. Pope (2002), Inverse modeling of partitioning interwell tracer tests: A streamline approach, *Water Resour. Res.*, *38*(6), 1079, doi:10.1029/2001WR000597.

Dugan, P. J., J. E. McCray, and G. D. Thyne (2003), Influence of a solubility-enhancing agent (cyclodextrin) on NAPL-water partition coefficients, with implications for partitioning tracer tests, *Water Resour. Res.*, *39*(5), 1123, doi:10.1029/2002WR001672.

Gottlieb, J., and P. Dietrich (1995), Identification of the permeability distribution in soil by hydraulic tomography, *Inverse Probl.*, *11*, 353–360.

Gutjahr, A. (1989), Fast Fourier transforms for random field generation, *N. M. Tech. Proj. Rep. Contract 4-R58-2690 R*, N. M. Inst. of Min. and Technol., Socorro.

Harter, Th., and T.-C. J. Yeh (1996), Conditional stochastic analysis of solute transport in heterogeneous, variably saturated soils, *Water Resour. Res.*, *32*(6), 1597–1610.

Harvey, C. F., and S. M. Gorelick (1995), Mapping hydraulic conductivity: Sequential conditioning with measurements of solute arrival time, hydraulic head, and local conductivity, *Water Resour. Res.*, *31*(7), 1615–1626.

James, A. I., W. D. Graham, K. Hatfield, P. S. C. Rao, and M. D. Annable (1997), Optimal estimation of residual non-aqueous phase liquid saturations using partitioning tracer concentration data, *Water Resour. Res.*, *33*(12), 2621–2636.

James, A. I., W. D. Graham, K. Hatfield, P. S. C. Rao, and M. D. Annable (2000), Estimation of spatially variable residual nonaqueous phase liquid saturations in nonuniform flow fields using partitioning tracer data, *Water Resour. Res.*, *36*(4), 999–1012.

Jin, M., M. Delshad, V. Dwarakanath, D. C. McKinney, G. A. Pope, K. Sepehrnoori, and C. E. Tilburg (1995), Partitioning tracer test for detection, estimation, and remediation performance assessment of subsurface nonaqueous phase liquids, *Water Resour. Res.*, *31*(5), 1201–1211.

Khachikian, C., and T. C. Harmon (2000), Nonaqueous phase liquid dissolution in porous Media: Current state of knowledge and research needs, *Transp. Porous Media*, *38*, 3–28.

Kitanidis, P. K. (1995), Quasi-linear geostatistical theory for inversing, *Water Resour. Res.*, *31*(10), 2411–2419.

Li, B., and T.-C. J. Yeh (1999), Cokriging estimation of the conductivity field under variably saturated flow conditions, *Water Resour. Res.*, *35*(12), 3663–3674.

Liu, S., T.-C. J. Yeh, and R. Gardiner (2002), Effectiveness of hydraulic tomography: Sandbox experiments, *Water Resour. Res.*, *38*(4), 1034, doi:10.1029/2001WR000338.

Liu, X., W. A. Illman, A. J. Craig, J. Zhu, and T.-C. J. Yeh (2007), Laboratory sandbox validation of transient hydraulic tomography, *Water Resour. Res.*, *43*, W05404, doi:10.1029/2006WR005144.

Mas-Pla, J., T.-C. J. Yeh, J. F. McCarthy, and T. M. Williams (1992), Numerical simulation of a two-well tracer experiment, *Ground Water*, *30*(6), 958–964.

McCarthy, J., B. Gu, L. Liang, J. Mas-Pla, T. M. Williams, and T.-C. J. Yeh (1996), Field tracer tests on the mobility of natural organic matter in a sandy aquifer, *Water Resour. Res.*, *32*(5), 1223–1238.

McDermott, C. I., M. Sauter, and R. Liedl (2003), New experimental techniques for pneumatic tomographical determination of the flow and transport parameters of highly fractured porous rock samples, *J. Hydrol.*, *278*(1–4), 51-63 JUL 25 2003.

Pankow, J. F., and J. A. Cherry (1996), *Dense Chlorinated Solvents and other DNAPLs in Ground water: History, Behavior, and Remediation*, 522 pp., Waterloo Press.

Rao, P. S. C., M. D. Annable, and H. Kim (2000), NAPL source zone characterization and remediation technology performance assessment: recent developments and applications of tracer techniques, *J. Contam. Hydrol.*, *45*, 63–78.

Renshaw, C. E. (1996), Estimation of fracture zone geometry from steady-state hydraulic head data using iterative sequential cokriging, *Geophys. Res. Lett.*, *23*(19), 2685–2688, SEP 1815.

Sciortino, A., T. C. Harmon, and W. W.-G. Yeh (2000), Inverse modeling for locating dense nonaqueous pools in groundwater under steady flow conditions, *Water Resour. Res.*, *36*(7), 1723–1736.

Sillan, R. K., M. D. Annable, P. C. C. Rao, D. P. Dai, K. Hatfield, W. D. Graham, A. L. Wood, and C. G. Enfield (1998), Evaluation of in situ cosolvent flushing dynamics using a network of multi-level samplers, *Water Resour. Res.*, *34*(9), 2191–2202.

Srivastava, R., and T.-C. J. Yeh (1992), A three-dimensional numerical model for water flow and transport of chemically reactive solute through porous media under variably saturated conditions, *Adv. Water Resour.*, *15*, 275–287.

Straface, S., T.-C. J. Yeh, J. Zhu, S. Troisi, and C. H. Lee (2007), Sequential aquifer tests at a well field, Montalto Uffugo Scalo, Italy, WRR, in review.

Sun, N. Z. (1994), *Inverse Problems in Groundwater Modeling*, pp. 103–140, Springer, New York.

Sun, N.-Z., and W. W.-G. Yeh (1990), Coupled inverse problems in groundwater modeling: 1. sensitivity analysis and parameter identification, *Water Resour. Res.*, *26*(10), 2507–2525.

Sykes, J. F., J. L. Wilson, and R. W. Andrews (1985), Sensitivity analysis for steady state groundwater flow using adjoint operators, *Water Resour. Res.*, *21*(3), 359–371.

Vargas-Guzman, A. J., and T.-C. J. Yeh (2002), The successive linear estimator: A revisit, *Adv. Water Resour.*, *25*, 773–781.

Vasco, D. W., H. Keers, and K. Karasaki (2000), Estimation of reservoir properties using transient pressure data: An asymptotic approach, *Water Resour. Res.*, *36*(12), 3447–3465.

Wu, C.-M., T.-C. J. Yeh, J. Zhu, T. H. Lee, N.-S. Hsu, C.-H. Chen, and A. F. Sancho (2005), Traditional analysis of aquifer tests: Comparing apples to oranges?, *Water Resour. Res.*, *41*, W09402, doi:10.1029/2004WR003717.

Yeh, T.-C. J., and S. Liu (2000), Hydraulic tomography: Development of a new aquifer test method, *Water Resour. Res.*, *36*(8), 2095–2105.

Yeh, T.-C. J., and J. Šimůnek (2002), Stochastic fusion of information for characterizing and monitoring the vadose zone, *Vadose Zone J.*, *1*, 207–221.

Yeh, T.-C. J., M. Jin, and S. Hanna (1996), An iterative stochastic inverse approach: conditional effective transmissivity and head fields, *Water Resour. Res.*, *32*(1), 85–92.

Yeh, T.-C. J., J. Mas-Pla, T. M. Williams, and J. F. McCarthy (1995a), Observation and three-dimensional simulation of chloride plumes in a sandy aquifer under forced-gradient conditions, *Water Resour. Res.*, *31*(9), 2141–2157.

Yeh, T.-C. J., A. L. Gutjahr, and M. H. Jin (1995b), An iterative cokriging-like technique for ground water flow modeling, *Ground Water*, *33*(1), 33–41, Jan.–Feb.

Zhang, Y., and W. D. Graham (2001), Spatial characterization of a hydrogeochemically heterogeneous aquifer using partitioning tracers: Optimal estimation of aquifer parameters, *Water Resour. Res.*, *37*(8), doi:10.1029/2000WR900377.

Zhu, J., and T.-C. J. Yeh (2005), Characterization of aquifer heterogeneity using transient hydraulic tomography, *Water Resour. Res.*, *41*, W07028, doi:10.1029/2004WR003790.

Zhu, J., and T.-C. J. Yeh (2006), Analysis of hydraulic tomography using temporal moments of drawdown recovery data, *Water Resour. Res.*, *42*, W02403, doi:10.1029/2005WR004309.

T.-C. J. Yeh and J. Zhu, Department of Hydrology and Water Resources, University of Arizona, John Harshbarger Building, 1133 E. North Campus Drive, Tucson, AZ 85721, USA. (ybiem@mac.hwr.arizona.edu)